MetUM-GOML: a near-globally coupled atmosphere–ocean-mixed-layer model

Article

Published Version

www.reading.ac.uk/centaur

CentAUR

Central Archive at the University of Reading

Geoscientific
Model Development

MetUM-GOML1: a near-globally coupled atmosphere–ocean-mixed-layer model

L. C. Hirons, N. P. Klingaman, and S. J. Woolnough

National Centre for Atmospheric Science-Climate and Department of Meteorology, University of Reading, P.O. Box 243, Reading, Berkshire, RG6 6BB, UK

Correspondence to: L. C. Hirons (l.c.hirons@reading.ac.uk)

Abstract. Well-resolved air–sea interactions are simulated in a new ocean mixed-layer, coupled configuration of the Met Office Unified Model (MetUM-GOML), comprising the MetUM coupled to the Multi-Column K Profile Parameterization ocean (MC-KPP). This is the first globally coupled system which provides a vertically resolved, high near-surface resolution ocean at comparable computational cost to running in atmosphere-only mode. As well as being computationally inexpensive, this modelling framework is adaptable – the independent MC-KPP columns can be applied selectively in space and time – and controllable – by using temperature and salinity corrections the model can be constrained to any ocean state.

The framework provides a powerful research tool for process-based studies of the impact of air–sea interactions in the global climate system. MetUM simulations have been performed which separate the impact of introducing interannual variability in sea surface temperatures (SSTs) from the impact of having atmosphere–ocean feedbacks. The representation of key aspects of tropical and extratropical variability are used to assess the performance of these simulations. Coupling the MetUM to MC-KPP is shown, for example, to reduce tropical precipitation biases, improve the propagation of, and spectral power associated with, the Madden–Julian Oscillation and produce closer-to-observed patterns of springtime blocking activity over the Euro-Atlantic region.

1 Introduction

Interactions between the atmosphere and ocean are a key feature of Earth's climate system, from instantaneous exchanges of heat, moisture and momentum to multi-decadal variability in large-scale, coupled circulations. By modifying the magnitude and direction of radiative and turbulent air–sea fluxes, variations in sea surface temperature (SST) can influence weather and climate globally (e.g. Sutton and Hodson, 2003; Giannini et al., 2003). However, it is not only interactions at the ocean surface which influence climate. The slower adjustment timescales within the upper ocean provide a source of predictability on seasonal timescales (e.g. the El Niño–Southern Oscillation (ENSO); Neelin et al., 1998), and basin-scale circulations within the deep ocean can drive multi-decadal variations in climate (Sutton and Hodson, 2005).

On subseasonal timescales, coupled feedbacks allow the atmospheric circulation to respond to and generate SST anomalies, largely through variations in surface fluxes (one-dimensional thermodynamics) rather than oceanic advection (three-dimensional dynamics). These high-frequency SST anomalies have been shown to influence the development and intensification of subseasonal phenomena such as the Madden–Julian Oscillation (MJO; e.g. Crueger et al., 2013), the monsoon onset (e.g. Prodhomme et al., 2014) and extratropical blocking (e.g. Pezza et al., 2012). A better understanding and simulation of how air–sea interactions influence these phenomena could improve subseasonal prediction and regional climate change projections.

1.1 The importance of air–sea interactions for weather and climate extremes

1.1.1 Air–sea interactions in the tropics

The dominant mode of subseasonal variability in the tropical atmosphere is the MJO (Madden and Julian, 1971), comprising eastward-propagating active and suppressed phases of convection in the tropical Indo-Pacific. The interaction between the atmosphere and ocean has been shown to influence the propagation of the MJO in an atmospheric general circulation model (AGCM) coupled to an idealised slab (e.g. Benedict and Randall, 2011) or a full dynamical ocean (e.g. DeMott et al., 2014) as well as in observations (Shinoda et al., 2013). Within the tropics, SST anomalies exhibit a near-quadrature phase relationship with rainfall: the peak warm (cold) SST leads the peak in enhanced (suppressed) convection by 7–10 days (Fu et al., 2003; Vecchi and Harrison, 2002). By inducing moistening downstream, this relationship is thought to be important for the propagation of organised tropical convection. However, AGCMs struggle to capture this observed phase relationship, often exhibiting collocated SST and rainfall anomalies (Rajendran et al., 2004). The observed near-quadrature phase relationship is reproduced in a coupled system (Rajendran and Kitoh, 2006), and results in a better simulation of the MJO (e.g. Woolnough et al., 2007; DeMott et al., 2014) as well as the northward-propagating Boreal summer intraseasonal oscillation (BSISO; e.g. Seo et al., 2007; Wang et al., 2009).

Air–sea interactions and the MJO also influence the onset and intraseasonal variability in the Asian (e.g. Lawrence and Webster, 2002), Australian (e.g. Hendon and Liebmann, 1990) and West African (e.g. Matthews, 2004) monsoons. For the Asian summer monsoon, the magnitude and gradients of SSTs in the Bay of Bengal and Indian Ocean are key to the formation of the onset vortex over the ocean which intensifies and moves northwards as the monsoonal circulation over land (Wu et al., 2012). Anomalous convection associated with the northward-propagating BSISO influences the active-break cycle of the Asian monsoon (e.g. Vitart, 2009; Klingaman et al., 2011). In the Australian pre-monsoon season, trade easterlies support a positive feedback between wind and SST resulting in strong persistent SST anomalies north of Australia. The monsoonal westerly regime, which is modulated by the propagation of the MJO active phase through the maritime continent (MC), causes this positive feedback to break down, weakening the SST anomalies significantly (Hendon et al., 2012). Oceanic warming around Africa can cause deep convection to migrate over the ocean, weakening the continental monsoon and leading to widespread drought from the Atlantic coast of western Africa to Ethiopia (Giannini et al., 2003). Equatorial warm pool SST anomalies associated with the MJO result in enhanced monsoonal convection over western and central Africa by forc-

ing eastward-propagating Kelvin and westward-propagating Rossby waves (Lavender and Matthews, 2009).

As well as influencing seasonal–subseasonal variability, air–sea interactions are key in determining the frequency and intensity of extreme events. Tropical cyclones, for example, are a strongly coupled phenomenon: they extract energy from the ocean and provide oceanic momentum, in the form of upwelling, which results in a cooling of the ocean surface below the cyclone centre. Ocean–atmosphere coupling in general circulation models (GCMs) has been shown to improve the spatial distribution of cyclogenesis (e.g. Jullien et al., 2014), as well as the representation of cyclone intensity (e.g. Sandery et al., 2010).

1.1.2 Air–sea interactions in the extratropics

There is also evidence that local high-frequency SST anomalies affect subseasonal variability in the extratropics. By altering meridional SST gradients, local anomalous SST patterns can affect the baroclinicity of the extratropical atmosphere (e.g. Nakamura and Yamane, 2009), resulting in persistent blocking conditions, intense heatwaves and droughts. For example, extreme heatwaves in southern Australia are typically induced and maintained by a blocking anticyclone that originates in the western Indian Ocean. An increased meridional SST gradient in the Indian Ocean, and hence enhanced baroclinicity, amplify upper-level Rossby waves which trigger heatwave conditions (Pezza et al., 2012). In summer 2003, warm SST anomalies in the northern Atlantic Ocean reduced the meridional SST gradient and decreased baroclinic activity, resulting in a northward shift of the polar jet and an expansion of the anticyclone and leading to an extreme heatwave over Europe (Feudale and Shukla, 2011). However, remote warm SST anomalies in the tropical Atlantic associated with anomalously wet conditions in the Caribbean Basin and the Sahel have also been suggested as a forcing for the 2003 heatwave (Cassou et al., 2005).

1.1.3 Tropical–extratropical teleconnections

Tropical–extratropical teleconnections suggest that remote, as well as local, air–sea interactions may be important to subseasonal variability. For example, tropical diabatic heating anomalies associated with the MJO can excite low-frequency wave trains which propagate into the extratropics in both hemispheres, affecting variations in the North Atlantic storm track and the frequency of blocking (Cassou, 2008). If GCMs accurately simulated both the MJO-associated tropical heating and the correct circulation response, this teleconnection could provide several weeks' predictability (Vitart and Molteni, 2010). The tropical–extratropical teleconnection is two-way: extratropical equatorward-propagating Rossby wave trains in the Southern Hemisphere can trigger convectively coupled Kelvin waves (Straub and Kiladis, 2003).

1.1.4 Frequency of air–sea interactions

The atmosphere and upper ocean interact instantaneously but many GCMs are only coupled once per day. Introducing diurnal coupling increases the variability in tropical SSTs which improves the amplitude of ENSO (Ham and Kug, 2010), causes an equatorward shift of the ITCZ (intertropical convergence zone) and a resulting stronger and more coherent MJO (Bernie et al., 2008), and improves the northward propagation of the BSISO (Klingaman et al., 2011). The impacts of subdaily coupling are not confined to the tropics but can affect the extratropics: including the ocean diurnal cycle decreased the meridional SST gradients in the North Atlantic resulting in a decrease in the zonal mean flow in the region (Guemas et al., 2013).

It is clear that interactions between the atmosphere and the ocean are important to a wide range of phenomena spanning many spatial and temporal scales. Section 1.2 will examine the current approaches to modelling air–sea interactions in global simulations.

1.2 Air–sea coupling in global climate models

Current widely used approaches for global simulations of climate are (1) AGCMs forced by prescribed SST and sea ice; (2) slab ocean experiments: an AGCM coupled to a simple one-layer thermodynamic ocean with either prescribed or interactive sea ice; and (3) coupled atmosphere–ocean general circulation models (AOGCMs) run with a full dynamical ocean and dynamic sea ice. Each approach has notable advantages and disadvantages. While (1) is computationally inexpensive and requires only an AGCM in which the desired SSTs and sea ice can be prescribed, the SST and ice boundary conditions cannot respond to variability in the atmosphere. This results in the wrong phase relationship between SST and rainfall anomalies (Fu et al., 2003; Rajendran and Kitoh, 2006) and can also lead to significant errors in the representation of phenomena for which air–sea interactions may be a critical mechanism (e.g. the MJO; Crueger et al., 2013).

In (2), the addition of a slab ocean permits thermodynamic processes to occur in the ocean. However, the slab ocean is not vertically resolved but typically comprises an $O(50\,\mathrm{m})$ thick layer. The SST response in slab models is often muted due to the slab's large thermal capacity and constant mixing depth. Studies have shown that fine upper-ocean vertical resolution allows coupled models to accurately represent subseasonal variations in mixed-layer depth and SST, which in turn enhances tropical subseasonal variability in convection and circulation (Woolnough et al., 2007; Klingaman et al., 2011; Tseng et al., 2014). Therefore, tropical subseasonal variability in a slab ocean model is very sensitive to the choice of mixing depth (e.g. Watterson, 2002). For example, slab ocean models with a very shallow (2 m) mixing depth have been shown to have a poor representation of

the MJO: the fast response of the atmosphere disables the wind-induced surface heat exchange (WISHE) mechanism (Maloney and Sobel, 2004). Furthermore, observations have shown that temperature and salinity anomalies stored beneath the mixing depth can reemerge and influence the atmospheric circulation in subsequent seasons (e.g. in the North Atlantic Bhatt et al., 1998; Alexander et al., 2000; Cassou et al., 2007). This mechanism is not present in a slab-coupled ocean model where the mixing depth cannot dynamically evolve.

In (3), both ocean dynamic and thermodynamic processes are represented so there is often no need to prescribe oceanic heat transports. However, the horizontal and vertical resolution of the AOGCM is limited by the computational expense of the ocean, especially if climate-length integrations are required. Furthermore, such models require long spin-up periods to attain a balance within the coupled system. They can also exhibit significant drifts and biases in the mean state, which can be of equal magnitude or larger than the desired signal (e.g. ENSO, decadal ocean variability, responses to greenhouse-gas or aerosol forcing). For example, many coupled models have a large cold equatorial SST bias in the tropical Pacific which inhibits their ability to simulate key modes of variability such as ENSO (Vannière et al., 2012).

1.3 Motivation for this study

Each of the modelling approaches described above is valuable and each, depending on the context, can be the most appropriate approach to answer a given set of scientific questions. However, there is a gap in the current modelling capability described in Sect. 1.2: no coupled system can provide a high-resolution, vertically resolved ocean at limited computational cost. The modelling framework described here addresses this gap.

This alternative approach is to couple an AGCM to a mixed-layer thermodynamic ocean model, comprised of one oceanic column below each atmospheric grid point. Previously, this has only been done in a handful of studies which do not use a contemporary AGCM, for example, studies coupling the Community Atmospheric Model version 2 (CAM2) to a 1-D ocean (e.g. Bhatt et al., 1998; Alexander et al., 2000; Cassou et al., 2007; Kwon et al., 2011). In this framework, because there is no representation of ocean dynamics, the mixed-layer model is computationally inexpensive ($<5\%$ of the cost of the atmosphere, as measured by CPU time[1]), which allows for higher near-surface vertical resolution and hence better-resolved upper-ocean vertical mixing than approach (2) and, in many cases, (3).

---

[1]The supercomputer used did not allow sharing one node between two executables. This reduces the efficiency of the coupled model, since one node must be devoted to OASIS and another to MC-KPP. Measured by wall-clock time, MetUM-GOML is approximately 25 % more expensive than the MetUM atmosphere at this horizontal resolution.

Therefore, within this coupled framework, well-resolved air–sea interactions are incorporated at comparable computational expense to approaches (1) and (2) but significantly cheaper than (3). This allows climate-length coupled integrations to be carried out at much higher atmospheric and oceanic horizontal resolutions than those currently achievable with (3).

One notable caveat of this framework is that temperature and salinity corrections must be prescribed, as in (2). While coupling to a mixed-layer model allows thermodynamic processes to occur in the ocean, corrections of temperature and salinity must be prescribed to represent the mean advection in the ocean and to correct for biases in AGCM surface fluxes. The method used to calculate and apply these corrections in this framework is described in Sect. 2.1.1. A further consequence of the lack of ocean dynamics is that the coupled model cannot represent modes of variability that rely on dynamical ocean processes (e.g. ENSO, AMO, PDO). However, depending on the application, this controllable feature of the framework could also be considered as an advantage. By adjusting the temperature and salinity corrections, the model can be easily constrained to any desired ocean state. When constrained to observations, for example, this results in much smaller mean SST biases compared with (3) (Fig. 1). This is important because the mean state is known to affect modes of variability (e.g. the MJO; Inness et al., 2003; Ray et al., 2011) and the perceived impact of coupling on that variability (Klingaman and Woolnough, 2014). Within this framework the role of air–sea interactions can be studied in a coupled model with the "right" basic state, thus, limiting the possibility that changes in the variability are a consequence of changes to the mean state. This feature of the coupled modelling system need not only be used to constrain to an observed ocean state, but could be exploited in further sensitivity studies (see discussion in Sect. 5).

As well as being controllable, this mixed-layer, coupled modelling framework has further technical advantages. It is very flexible: because the ocean comprises independent columns below each atmospheric grid point, air–sea coupling can be selectively applied in space and time. This provides a test bed for sensitivity studies to understand the relative role of local and remote air–sea interactions and how they feed back onto atmospheric variability. Furthermore, the framework is very adaptable: the coupling can be applied to any GCM at its own resolution.

The coupled atmosphere–ocean-mixed-layer model configuration, and the simulations which have been performed, are described in Sect. 2. The impact of well-resolved air–sea interactions are evaluated within those simulations in terms of the mean state (Sect. 3) and aspects of tropical (Sect. 4.1) and extratropical (Sect. 4.2) variability. These results are summarised in Sect. 5 along with a discussion of potential further applications of this modelling capability.
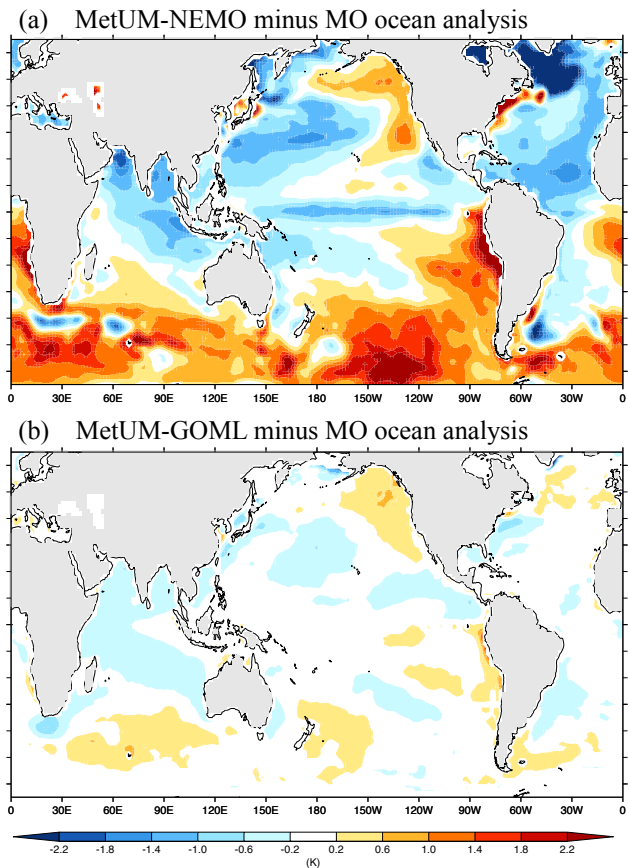

Figure 1. Annual-mean SST bias compared with the Met Office (MO) ocean analysis (Smith and Murphey, 2007). **(a)** 30 years of the Met Office Unified Model AGCM (MetUM) coupled to a full dynamical ocean, NEMO. **(b)** 60 years of a free-running MetUM-GOML simulation: the MetUM coupled to the multi-column mixed-layer ocean model, MC-KPP. The flux corrections in this MetUM-GOML simulation are calculated as described in Sect. 2.2.

2 Model, methods and data

The near-globally coupled atmosphere–ocean-mixed-layer model is described here, first in terms of the general framework (Sect. 2.1) and then the specific implementation of that framework to the Met Office Unified Model, as used for the experiments in this study (Sect. 2.2).

2.1 The new coupled modelling framework

The coupled modelling framework comprises an AGCM coupled to the Multi-Column K Profile Parameterization (MC-KPP) mixed-layer ocean model via the Ocean Atmosphere Sea Ice Soil (OASIS) coupler (Valcke et al., 2003). MC-KPP is run as a two-dimensional matrix of 1-D water columns, with one column below each AGCM grid point that is wholly or partially ocean. The effective horizontal resolution of MC-KPP is, therefore, the same as the AGCM to which it is coupled. The vertical discretization of the MC-

KPP columns is defined using a stretch function, allowing very high resolution in the upper ocean. Vertical mixing in MC-KPP is parameterised using the KPP scheme of Large et al. (1994). KPP includes a scheme for determining the mixed-layer depth by parameterising the turbulent contributions to the vertical shear of a bulk Richardson number. A nonlocal vertical diffusion scheme is used in KPP to represent the transport of heat and salt by eddies with a vertical scale equivalent to that boundary-layer depth.

Outside the chosen coupling domain, the AGCM is forced by daily climatological SSTs and sea ice from a reference climatology. At the coupling boundary a linear interpolation blends the coupled and reference SSTs and sea ice to remove any discontinuities. A regionally coupled configuration of this framework, with coupling in the tropical Indo-Pacific, is described in Klingaman and Woolnough (2014).

2.1.1 Flux-correction technique

Flux corrections or adjustments have long been used to remove climate drift from coupled GCMs (Sausen et al., 1988). Since MC-KPP simulates only vertical mixing and does not represent any ocean dynamics, depth-varying temperature and salinity corrections are required to represent the mean ocean advection and account for biases in atmospheric surface fluxes. The corrections are computed in a "relaxation" simulation in which the AGCM is coupled to MC-KPP, and the MC-KPP profiles of temperature and salinity are constrained to a reference climatology with a relaxation timescale τ. These correction terms are output as vertical profiles of temperature and salinity tendencies. The reference climatology to which the model is constrained could be taken from an ocean model or from an observational data set. The daily mean seasonal cycle of temperature and salinity corrections from the constrained coupled "relaxation" simulation are then imposed in a free-running coupled simulation with no interactive relaxation.

When corrections are calculated by constraining ocean temperature and salinity profiles to an observational reference climatology with $\tau = 15$ days, the resulting free-running, coupled simulation in which those corrections are applied produces small SST biases compared with observations (Fig. 1b). Furthermore, the global SSTs in the free-running, coupled simulation show no signs of drift within in the 20 years of each individual simulation.

2.2 The near-globally coupled MetUM-GOML configuration

The ocean mixed-layer, coupled framework described above has been applied to the Met Office Unified Model (MetUM-GOML; see details in Sect. 2.3) with 3-hourly coupling between the atmosphere and ocean. The simulations discussed in the current study are run at $1.875°$ longitude $\times$ $1.25°$ lati-
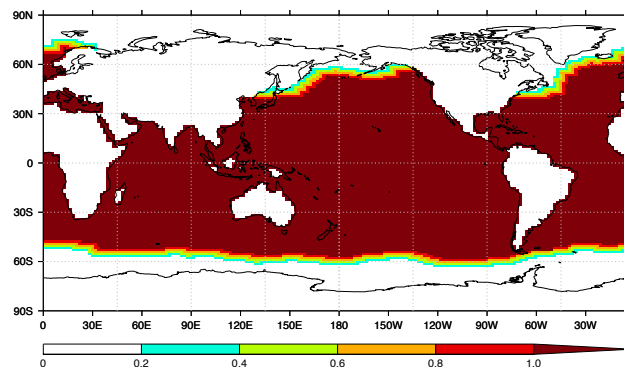

Figure 2. Coupling mask showing the five-grid-point linear blend between the MetUM-GOML coupling region ($\alpha = 1$; dark red) and the SST boundary condition outside the coupling region ($\alpha = 0$; white).

tude horizontal resolution with 85 points in the vertical and a model lid at 85 km.

In MetUM-GOML the MetUM and MC-KPP have been coupled nearly globally as shown in Fig. 2. The latitudinal extent of the MetUM-GOML coupling domain has been determined taking into account regions of seasonally varying sea ice because MC-KPP does not include a sea ice model. This was done using the sea ice data set from the Atmospheric Model Intercomparison Project (AMIP) component of the Coupled Model Intercomparison Project phase 5 (Taylor et al., 2012): coupling was not applied at points which had 30 days year^{-1} of ice for ≥ 3 years in the data set. Finally, the resulting coupling edge was smoothed to create the near-globally coupled MetUM-GOML domain (Fig. 2). Outside the coupled region, the MetUM is forced by daily climatological (1980–2009) SSTs from the Met Office ocean analysis (Smith and Murphey, 2007) and sea ice from the AMIP data set (Taylor et al., 2012), with a five-grid-point linear blend at the boundary.

In the current study, MC-KPP is configured with a depth of 1000 m over 100 vertical levels; previous tropical simulations only required a depth of 200 m (Klingaman et al., 2011). Test simulations were carried out to define an appropriate depth for the near-globally coupled MetUM-GOML to ensure that the maximum depth of the mixed layer remained less than the total depth of the MC-KPP columns. High near-surface resolution is maintained by using a stretch function for the first 72 vertical levels (287.2 m). The vertical resolution is 1.2 m at the surface, less than 2 m over the first 41.5 m and less than 5 m to a depth of 127.8 m. Below 287.2 m the remaining levels are equally spaced every 25.0 m to the depth of 987.2 with a final lower level at 1000 m. Bathymetry is defined using the ETOPO2 Global Relief Model from NOAA (Smith and Sandwell, 1997) interpolated to the MetUM-GOML horizontal grid. Where the ocean depth is < 1000 m, MC-KPP is prevented from computing a mixed-layer depth greater than the ocean depth.

The depth-varying temperature and salinity corrections were computed from a 10-year, coupled MetUM-GOML integration (K-O-RLX) in which 3-D profiles of salinity and temperature were strongly constrained to the Met Office ocean analysis (Smith and Murphey, 2007) with a 15-day relaxation timescale τ. The mean seasonal cycle of tendencies from K-O-RLX are then imposed in free-running MetUM-GOML simulations (Sect. 2.3). Different choices of τ were tested (e.g. 5, 15, 30, and 90 days) to find a suitable timescale which sufficiently constrained the salinity and temperature profiles without damping subseasonal variability. A 15-day relaxation timescale was chosen because it produced the smallest SST biases in the free-running, coupled simulation. Longer timescales produced larger SST biases since the relaxation was too weak to counter the SST drift, which arises from the lack of ocean dynamics and biases in atmospheric surface fluxes. With the shorter (5-day) timescale, the atmospheric surface fluxes did not adequately adjust to the presence of coupling in the relaxation simulation. This led to a substantial difference between the surface-flux climatologies of the free-running and relaxation simulations, for which the temperature and salinity tendencies could not correct, and hence larger SST biases than the simulation in which the 15-day relaxation was used.

2.3 Experimental setup

All experiments in the present study use the MetUM AGCM at the fixed scientific configuration Global Atmosphere 3.0 (GA3.0; Arribas et al., 2011; Walters et al., 2011). Coupled simulations use the ocean mixed-layer, coupled configuration MetUM-GOML1, comprising the MetUM GA3.0 coupled to MC-KPP1.0 (as described above). The experiments are labelled in the form (experiment type) − (ocean condition), where experiment type describes whether the MetUM is coupled to MC-KPP ("K") or run in atmosphere-only mode ("A"). The ocean condition describes either the data set to which the simulation is constrained, in the case of coupled simulations, or the SST boundary condition used to force the atmosphere-only simulations. The coupled simulations here are constrained to the mean seasonal cycle (1980–2009) of observed ("O") ocean temperature and salinity from the Met Office ocean analysis (Smith and Murphey, 2007; Fig. 2).

To test this model configuration and investigate the role of well-resolved upper-ocean coupling, three sets of experiments have been conducted. K-O describes the free-running MetUM-GOML simulations in which the climatological temperature and salinity corrections from the strongly constrained K-O-RLX simulation are applied. Three K-O simulations have been run for 25 years each, initialised from 1 January of year 10, 9 and 8 of the 10-year K-O-RLX simulation, respectively. The coupled integrations are compared with two sets of atmosphere-only simulations forced by (a) the daily mean seasonal cycle of SSTs averaged over 60 years of K-O (years 6–25 of each K-O simulation): A-Kcl,

and (b) 31-day smoothed SSTs from the three K-O simulations: A-K31. The A-K31 experiment is designed to mimic the AMIP-style setup of forcing with monthly-mean SSTs. A 31-day running mean produces a smoother SST time series than interpolating monthly means to daily values. The initialisation and run length of the A-Kcl and A-K31 simulations are identical to those of the K-O simulations. The first five years of each simulation have been excluded from the analysis, and the following 20 years (years 6–25) contribute to the results shown here. Therefore, 60 years from each experiment have been analysed. The experiments are summarised in Table 1.

In this experimental setup the impact of introducing interannual variability in SSTs (A-K31 minus A-Kcl) can be separated from the impact of coupling feedbacks (K-O minus A-K31; Table 2) within a model that, by construction, has a close-to-observed basic state. However, since the K-O SSTs used to force A-K31 have undergone a 31-day smoothing, the latter comparison (K-O minus A-K31) includes the effect of sub-31-day SST variability as well as the impact of coupling feedbacks.

2.4 Observational data sets

The evaluation of the mean state (Sect. 3) and tropical and extratropical variability (Sect. 4) in the MetUM simulations is made through comparisons with three observational data sets. Daily instantaneous (00Z), pressure-level specific humidity, zonal wind, temperature and geopotential height data are taken from the European Centre for Medium-range Weather Forecasts Interim reanalysis (ERA-Interim; Dee et al., 2011) for 1990–2009. Rainfall data are taken from the Tropical Rainfall Measuring Mission (TRMM; Kummerow et al., 1998) 3B42 product, version 6, for 1999–2011 on a $0.25° × 0.25°$ grid. Outgoing longwave radiation (OLR) data are taken from the National Oceanic and Atmospheric Administration (NOAA) Advanced Very High Resolution Radiometer (AVHRR) data set for 1989–2009 on a $2.5° × 2.5°$ grid. Where direct comparisons are made between the MetUM and ERA-Interim and TRMM, the observational data have been interpolated to the MetUM grid using an area-weighted interpolation method. Where comparisons have been made with NOAA data, the MetUM simulations have been interpolated to the NOAA grid.

3 Impact of air–sea interactions on the mean state

The underlying mean state of a GCM is known to influence the representation of various modes of variability within that model. All of the simulations described in this study have the same mean seasonal cycle of SSTs, and therefore it is expected that the mean state of these simulations will be similar. However, there may be changes in variability that feed back on the mean state.

Table 1. Summary of simulations carried out in the current study.

Experiment	Coupling	Ocean condition	Simulations×years
K-O	MC-KPP near-global (K)	Mean seasonal cycle from observations (O; Smith and Murphey, 2007)	3 × 25
A-K31	Atmosphere-only (A)	31-day smoothed K-O (K31)	3 × 25
A-Kcl	Atmosphere-only (A)	Mean seasonal cycle from K-O (Kcl)	3 × 25

Table 2. Focus comparisons of experiments in the study and the impacts revealed by each.

Comparison	Impact of
K-O minus A-K31	Coupling feedbacks
A-K31 minus A-Kcl	Interannual variability in SST
K-O minus A-Kcl	Combined effect

3.1 Zonal-mean vertical structure

Analysing the annual-mean zonal-mean vertical structure of temperature and specific humidity shows that the MetUM is more than $1\,\mathrm{g\,kg^{-1}}$ too dry in the tropical lower-troposphere (not shown), up to $4\,°C$ too warm throughout the stratosphere and up to $2\,°C$ too cold in much of the troposphere (Fig. 3a) compared with ERA-Interim reanalysis. These differences are not seasonally dependent, although the tropospheric cooling is stronger in the Northern Hemisphere during winter and spring.

Compared with A-Kcl, K-O warms and dries the tropical lower-troposphere by approximately $0.6\,\mathrm{K}$ (Fig. 3b) and $0.4\,\mathrm{g\,kg^{-1}}$ (not shown), respectively, while the stratosphere in the Southern (Northern) Hemisphere is cooled (warmed) slightly (Fig. 3b). These changes in the zonal-mean vertical structure of temperature and specific humidity are a result of the coupling feedbacks in K-O (Fig. 3d) rather than the introduction of interannual variability in SST in the atmosphere-only configuration (A-K31; Fig. 3c). The inclusion of air–sea interactions has the added impact of slightly cooling the tropical upper troposphere (Fig. 3d) which suggests that overall convection is slightly shallower in K-O compared with A-K31.

The upper-level subtropical jets in the MetUM are shifted equatorward compared with ERA-Interim (Fig. 4a), particularly in the Northern Hemisphere. This results in a tropical westerly bias at upper-levels compared with ERA-Interim. In K-O, the subtropical jet in the Southern Hemisphere is narrowed and the magnitude of the equatorial upper-level westerly bias is reduced (Fig. 4b). These changes are a consequence of the introduction of interannual variability in SST (Fig. 4c) and the air–sea coupling feedbacks (Fig. 4d), respectively.

3.2 Precipitation

Compared with TRMM all MetUM simulations exhibit wet annual-mean precipitation biases over the equatorial Indian Ocean (IO) and the South Pacific convergence zone (SPCZ) and dry annual-mean precipitation biases over the Indian subcontinent, Australia and the MC islands (Fig. 5b). This is a long-standing and well-documented bias in the MetUM (e.g. Ringer et al., 2006), which was also present in CMIP3 models and not improved in CMIP5 (Sperber et al., 2013). Figure 5c shows the tropical precipitation biases in the fully coupled MetUM-NEMO configuration. While they are of similar magnitude to those in A-K31, they differ in their spatial distribution: in MetUM-NEMO the equatorial IO bias is focused in the western IO and a dry bias is present in the western Pacific warm pool region (Fig. 5c). These differences are a result of different biases in SST in the MetUM-GOML model compared with MetUM-NEMO (Fig. 1). Compared with the MetUM-NEMO configuration, A-K31 increases precipitation in the central IO and equatorial Pacific and reduces precipitation in the western IO and off-equatorial regions of the Pacific (Fig. 5d).

Coupling the MetUM to MC-KPP reduces this precipitation bias by drying the equatorial IO and SPCZ and increasing precipitation over the MC islands; however, little improvement is made to the significant dry biases over continental India. Introducing interannual variability in SST can account for most of the reduction in rainfall over the equatorial IO (Fig. 5e) but has little impact in the Pacific. Conversely, the reduction of the wet bias in the SPCZ is a consequence of the coupling feedbacks (Fig. 5f). Over the MC region interannual variability in SST and coupling feedbacks have opposite drying and moistening effects respectively.

This precipitation bias in the MetUM is particularly pronounced during the Asian summer monsoon season during which it exhibits weaker-than-observed upper-level winds and deficient (excess) precipitation over India (the equatorial IO; Ringer et al., 2006). During JJA, the wet precipitation bias over the central IO in K-O is reduced by more than $5\,\mathrm{mm\,day^{-1}}$, largely as a result of the interannual variability in SST introduced in A-K31 (Fig. 5g). Little improvement is made in K-O to the lack of monsoonal precipitation over the Indian subcontinent (Fig. 5g, h).

While the mean state has been shown to differ slightly between K-O, A-K31 and A-Kcl, these changes are small in magnitude. The simulations have the same mean SST pat-
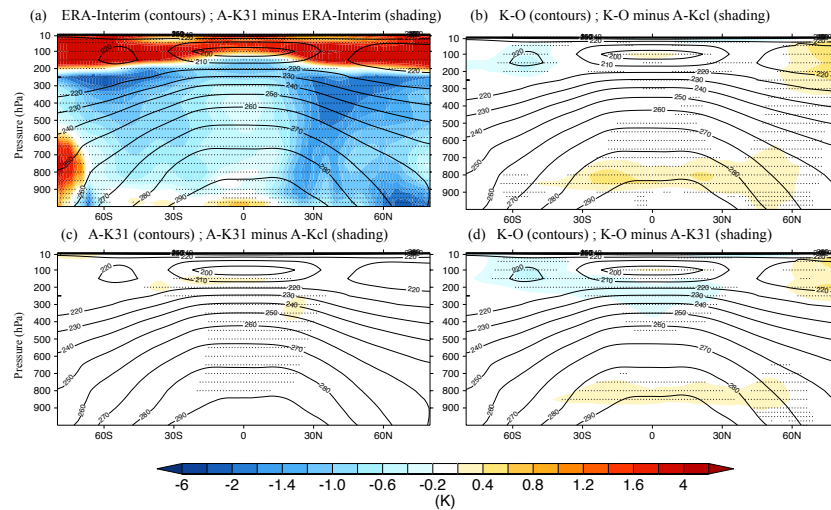
Figure 3. (a) Annual-mean zonal-mean temperature from the ERA-Interim (contours) and bias of A-K31 compared with the ERA-Interim (shading). Impact of interannual SST variability (**c**; A-K31 minus A-Kcl), coupling (**d**; K-O minus A-K31) and both SST variability and coupling (**b**; K-O minus A-Kcl) on the vertical structure of zonal-mean temperature. Stippling indicates where differences are significant at the 95 % level.
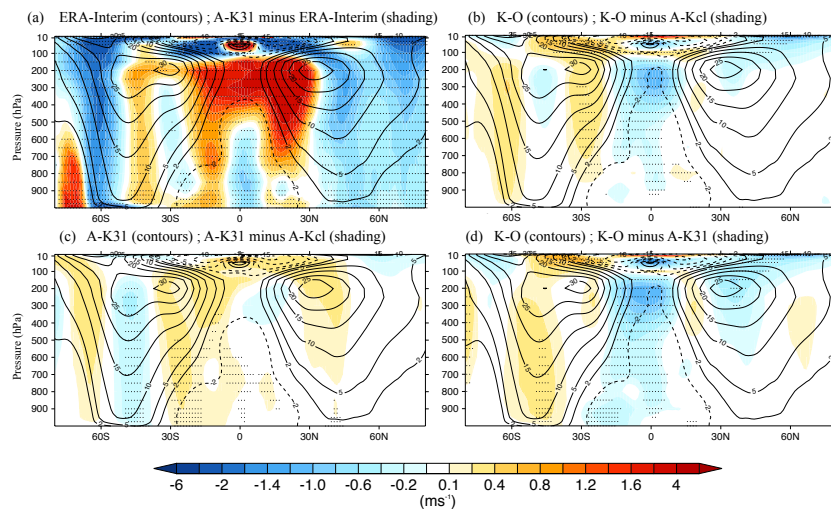

Figure 4. As in Fig. 3, but for the annual-mean zonal-mean zonal wind.

terns which, by constraining the K-O ocean temperature and salinity, is close to observations. This allows changes in the variability (Sect. 4) within this modelling framework to be attributed to the impact of introducing interannual variability in SST (A-K31 minus A-Kcl) or having air–sea interactions (K-O minus A-K31), rather than to changes in the basic state of the model.

4 Impact of coupling on variability

Teleconnections between the tropics and extratropics suggest that remote and local air–sea interactions are important to the representation of variability on subseasonal timescales

(Sect. 1.1.3). Aspects of both tropical (Sect. 4.1) and extratropical (Sect. 4.2) variability will be examined in the current simulations.

4.1 Tropical variability

To investigate the role of air–sea interactions on the representation of variability in the tropics, the analysis has focused on the representation of convectively coupled equatorial waves (Sect. 4.1.1) and the Madden–Julian Oscillation (Sect. 4.1.2).
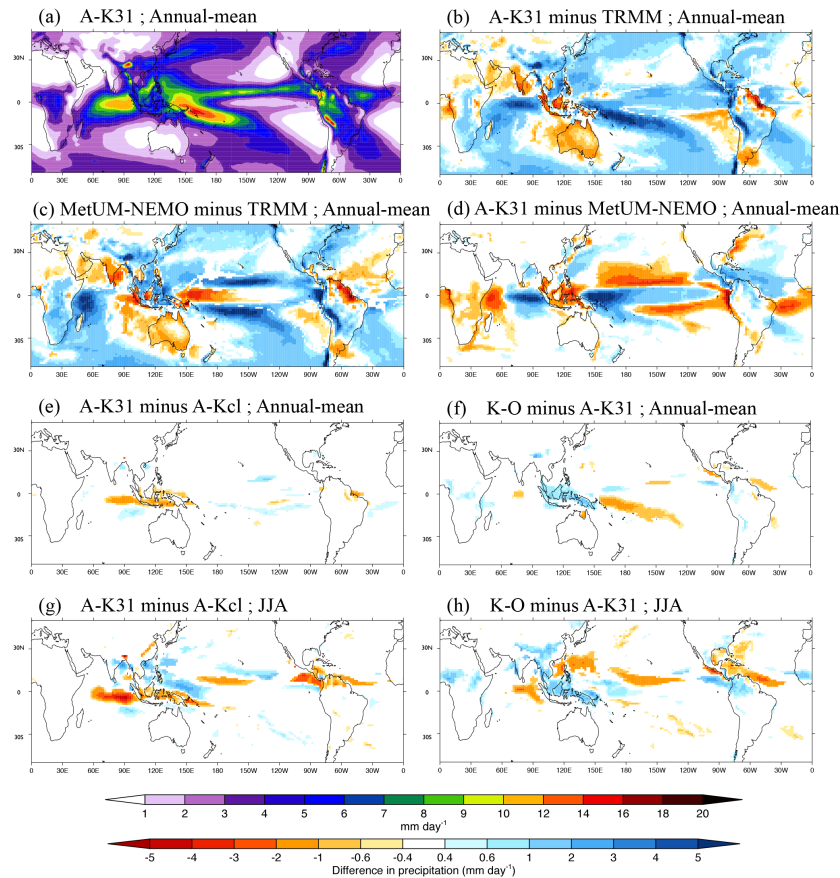
Figure 5. (a) Annual-mean precipitation from A-K31. **(b and c)** show the annual-mean bias of A-K31 and MetUM-NEMO against TRMM satellite observations. **(d)** Change of annual-mean precipitation between A-K31 and MetUM-NEMO. Impact of introducing interannual variability in SST (**e, g**; A-K31 minus A-Kcl) and having air–sea interactions (**f, h**; K-O minus A-K31) on annual-mean and JJA (June-July-August) precipitation, respectively. Differences are only shown where they are significant at the 95 % level.

4.1.1 Convectively coupled equatorial waves

A substantial proportion of large-scale organised tropical convection is associated with equatorial waves. Therefore, it is important to examine how these wave modes are represented in these simulations. The organisation of tropical convection by equatorial waves is examined by computing the space–time power spectra of anomalous, equatorially averaged (15° N–15° S) OLR, as in Wheeler and Kiladis (1999). After computing tropical OLR anomalies from the seasonal cycle, the zonal wave number-frequency power spectra are separated into symmetric and antisymmetric components and the red background spectrum removed. This results in the emergence of preferred space and timescales for organised tropical convection. In NOAA satellite observations these preferred scales are consistent with theoretical equatorial waves, highlighted by the dispersion curves at varying equivalent depths (solid lines). For example, in the observed symmetric spectrum, eastward-propagating Kelvin and westward-propagating equatorial Rossby (ER) waves emerge, as well as a signature of the eastward-propagating

intraseasonal MJO at zonal wave numbers 1–3 (Fig. 6a). In the antisymmetric component the observations exhibit power associated with mixed Rossby-gravity (MRG) and eastward-propagating inertio-gravity (EIG) waves (Fig. 6e).

The variability associated with these equatorial wave modes in the MetUM is considerably weaker than in observations. All MetUM simulations exhibit symmetric power associated with Kelvin- and ER-wave modes. However, variance associated with the antisymmetric MRG and inertio-gravity-wave modes is almost entirely absent (Fig. 6f–h). In A-Kcl, low-frequency tropical wave activity is not confined to low zonal wave numbers, as in observations (±5), but extends to westward wave number 10 and eastward wave number 15 (Fig. 6b). Introducing interannual variability in SST has little impact on this overestimation of low-frequency power. In K-O, air–sea interactions result in the low-frequency power being confined to smaller westward wave numbers (Fig. 6d), which is more consistent with observations (Fig. 6a). The dominant mode in the OLR spectrum within the eastward wave number 1–3 band and the 30–80-day frequency range is the MJO. Figure 6d suggests that air–sea interactions in-
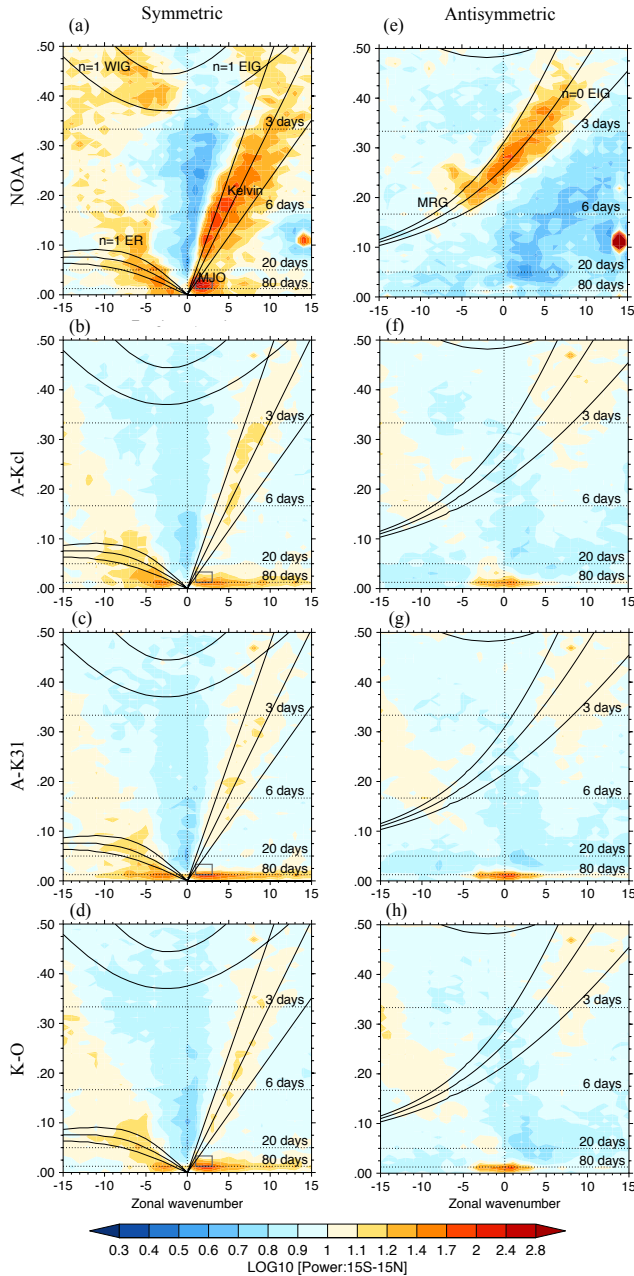
Figure 6. Zonal wave number-frequency power spectra of anomalous OLR for symmetric **(a–d)** and antisymmetric **(e–h)** components divided by the background power for NOAA satellite observations **(a, e)**, A-Kcl **(b, f)**, A-K31 **(c, g)** and K-O **(d, h)**. Solid lines represent dispersion curves at equivalent depths of 12, 25 and 50 m. Theoretical modes highlighted in observations: ER, Kelvin, MRG, and eastward and westward inertio-gravity (EIG, WIG). The grey box indicates the MJO spectral region of 30–80 days and wave numbers 1–3.

crease the magnitude of MJO power and slightly broaden that power over a wider frequency range. As a complex, multi-scale phenomenon the MJO, and teleconnection patterns associated with it, acts as a rigorous test for GCMs and hence its representation in these simulations warrants further investigation (Sect. 4.1.2).

4.1.2 The Madden–Julian Oscillation

Intraseasonal variability in the tropical atmosphere–ocean system is dominated by the MJO (e.g. Madden and Julian, 1972; Zhang, 2005). The active phase of the MJO can be characterised as a planetary-scale envelope of organised deep convection which propagates eastward from the Indian Ocean into the western Pacific. Ahead and behind the deep convective centre are areas of suppressed convection. The active and suppressed phases of the MJO are connected by a strong overturning circulation in the zonal wind. Significant effort has gone into defining indices and diagnostics which fully describe the representation of the MJO in observations and model simulations (e.g. Wheeler and Hendon, 2004; Kim et al., 2009).

One such diagnostic is to extract variability associated with the MJO by bandpass filtering fields, such as precipitation, to MJO timescales (e.g. 20–80 days). The standard deviation in 20–80-day filtered precipitation from A-K31 shows maxima in variability located over the equatorial Indo-Pacific (Fig. 7a). Comparison with TRMM satellite data shows that the A-K31 overestimates intraseasonal variability in precipitation over the equatorial IO, SPCZ, southern Africa and north of Australia (Fig. 7b); this is consistent with the overestimation of the mean precipitation in these regions (Fig. 5). Conversely, intraseasonal variability in precipitation is underestimated in A-K31 over the Gulf of Guinea and the Indian subcontinent. Introducing interannual variability in SST has little impact on these biases in the variability of intraseasonal precipitation (Fig. 7b). Including air–sea interactions in K-O generally reduces intraseasonal variability in precipitation over the equatorial oceans and increases variability over central Africa and India (Fig. 7d). These changes in variability result in a better representation of intraseasonal precipitation in K-O; this is also consistent with the mean-state change in precipitation shown in Fig. 5.

To assess the zonal propagation of the MJO in the MetUM, lag regressions of latitude-averaged (15° N–15° S), 20–80-day bandpass filtered precipitation are computed using three base points: in the central Indian Ocean (70° E), the western edge of the maritime continent (100° E) and the western Pacific (130° E). This is a further diagnostic recommended by the CLIVAR MJO Task Force (Kim et al., 2009), which has previously been applied to MJO-filtered OLR to investigate the role of local air–sea interactions in the MetUM GA3.0 (Klingaman and Woolnough, 2014).

TRMM observations (Fig. 8a–c) show clear eastward propagation of the active and suppressed phases of the MJO
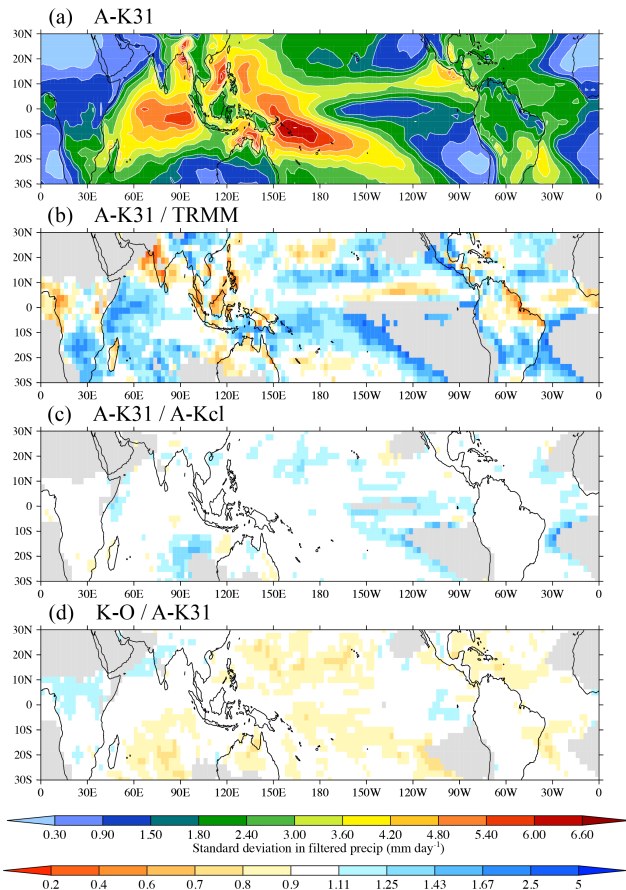
Figure 7. Standard deviation in 20–80-day filtered precipitation from **(a)** A-K31. Ratio of standard deviations from A-K31 and TRMM **(b)**, A-K31 and A-Kcl **(c**; impact of SST variability) and K-O and A-K31 **(d**; impact of coupling). In **(b–d)**, regions with a standard deviation of filtered precipitation below 1 mm day^{-1} have been excluded from the ratio calculation and masked grey.

along the dashed line which represents the approximate observed phase speed of the MJO. In A-Kcl, subseasonal variability in precipitation is either stationary or propagates to the west (Fig. 8d–f). Introducing interannual variability in SST in A-K31 reduces the extent of westward propagation of subseasonal precipitation, especially over the maritime continent (Fig. 8h compared with Fig. 8e). The eastward propagation of subseasonal variability in precipitation is only achieved with the inclusion of air–sea interactions in K-O (Fig. 8j–l). Although the magnitude of the anomalies remain weaker than observed, K-O is able to produce anomalies which propagate at the correct phase speed (compared with dashed line). The transition from westward-propagating (in A-Kcl and A-K31) to eastward-propagating (in K-O) intraseasonal precipitation anomalies is especially striking over the maritime continent (base point 100° E; Fig. 8e, h, k), a region in which models typically struggle to maintain the MJO signal (e.g. Vitart and Molteni, 2009). The impact of air–sea interactions on

the eastward propagation of the MJO here within the near-globally coupled MetUM-GOML is consistent with a similar MetUM mixed-layer ocean coupled simulation with coupling only in the Indo-Pacific (Klingaman and Woolnough, 2014).

It is clear that air–sea interactions play an important role in the representation of tropical subseasonal variability. Specifically, K-O has shown a distinct improvement in the representation of tropical variability associated with the MJO. However, deficiencies remain in the simulation of MJO activity in K-O. While air–sea interactions have improved the propagation of the MJO in the MetUM (Fig. 8), the amplitude of MJO activity remains significantly weaker than in observations (Fig. 6). Existing studies suggest that MJO-related tropical heating anomalies can excite wave trains which propagate polewards and modulate aspects of variability in the extratropics (e.g. Cassou, 2008). If the improvements in MJO activity are large enough and the MetUM is able to accurately represent the circulation response to the MJO then, through this tropical–extratropical teleconnection, changes may also be expected in the representation of the extratropical variability in K-O. This is examined in Sect. 4.2 through investigation of the Northern Hemisphere storm tracks and blocking frequency.

4.2 Extratropical variability

Analysis of the role of air–sea interactions on the representation of extratropical variability is focused on the Northern Hemisphere storm tracks and blocking.

4.2.1 Northern Hemisphere storm tracks

Daily variability in the Northern Hemisphere midlatitudes is largely controlled by the Atlantic and Pacific storm tracks. Cyclones originating in the western Atlantic and Pacific oceans move east along a preferred path or storm track, bringing significant precipitation and strong winds to Europe and North America. Because variations in these storm tracks modulate the continental climate of the Northern Hemisphere, their representation in GCMs is important.

Previous analyses of storm track activity in GCMs fall into two broad categories: feature tracking of weather systems (e.g. Hoskins and Hodges, 2002) and 2–6-day bandpass filtering (e.g. 500 hPa geopotential height; Blackmon, 1979). The application of these techniques within coupled and atmosphere-only configurations of the MetUM yield broadly consistent results (Martin et al., 2004). Here, the latter is applied: 24-hourly instantaneous geopotential heights at 500 hPa are bandpass filtered between 2 and 6 days. This method isolates the high-frequency eddy activity in the mid-troposphere, which, by identifying the passage of synoptic weather systems, is a reliable indication of the location of the storm tracks.

Figure 9a shows the standard deviation of the wintertime (DJF – December-January-February) 2–6-day bandpass-
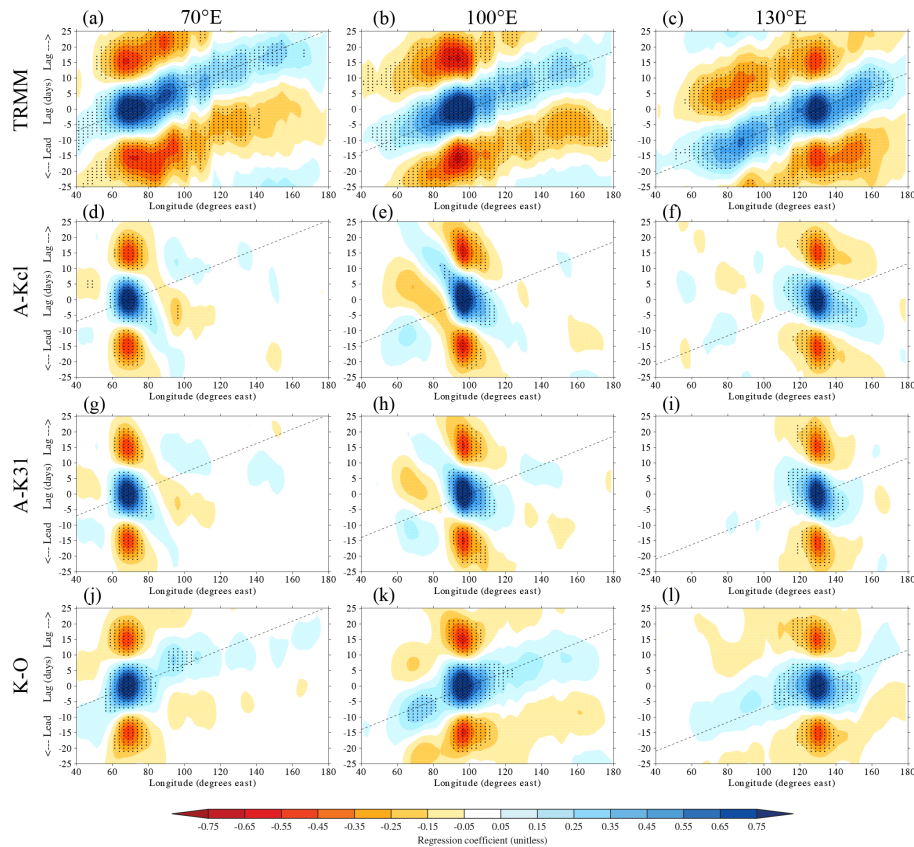
Figure 8. Lag regressions of latitude-averaged (15° N–15° S), 20–80-day bandpass-filtered precipitation against base points in the central Indian Ocean (70° E; **a, d, g, j**), maritime continent (100° E; **b, e, h, k**) and western Pacific (130° E; **c, f, i, l**). Positive and negative days represent lags and leads, respectively. Approximate observed propagation speeds are shown by the dashed lines. Stippling indicates where the lag regressions are significant at the 95 % level.

filtered geopotential heights at 500 hPa from A-K31 in the Northern Hemisphere. There are two clear areas of activity over the midlatitude Pacific and Atlantic ocean basins, with the eddy activity maxima, where cyclogenesis is most common, over the west of the respective basins. The overall location of the storm tracks in the MetUM is similar to ERA-Interim, with eddy maxima occurring in the right place. There is a slight equatorward bias in the storm tracks over the ocean compared with ERA-Interim (Fig. 9b, c) which is consistent with the equatorward shift of the Northern Hemisphere subtropical jet seen in Fig. 4a. In the MetUM there is generally not enough eddy activity; the Atlantic storm track does not extend far enough into Europe, and the Pacific track is too weak (Fig. 9b, c). Introducing interannual variability in SST slightly broadens the area of strong eddy activity into the northern Pacific but has little impact on the extension of the Atlantic track into Europe (Fig. 9d). Introducing air–sea interactions in K-O has little impact on the representation of the Pacific and Atlantic storm tracks compared with A-K31 (Fig. 9e). The limited impact on the Northern Hemisphere storm tracks in K-O suggests that the improvements in tropical intraseasonal variability may not be sufficiently large to

influence extratropical variability, at least by this measure. It may also be that horizontal resolution plays a role; the simulations shown here may be too coarse to sufficiently capture the extratropical variability, no matter how well the tropical intraseasonal variability is represented.

4.2.2 Northern Hemisphere blocking

On synoptic scales persistent high-pressure systems, or atmospheric blocking, are key in modulating weather extremes in the midlatitudes and therefore an important feature for GCMs to capture realistically. Climate models typically underestimate blocking frequency (Scaife et al., 2010), irrespective of the index used to describe the phenomena (Doblas-Reyes et al., 2002). Here, Euro-Atlantic blocking is identified using an absolute geopotential height index described in Scherrer et al. (2006), which is an extension of that of Tibaldi and Molteni (1990). Linear gradients of 500 hPa geopotential height are calculated 15° north and south of central latitudes between 35 and 75° N. A particular grid point is considered blocked if the southern gradient is reversed and the northern gradient is less than -10 m per degree of lat-
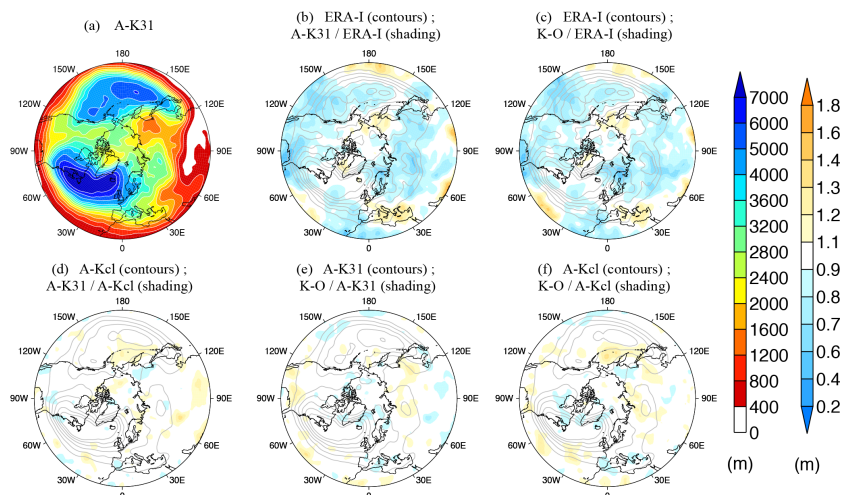
Figure 9. Standard deviation in wintertime (DJF) 2–6-day bandpass-filtered 500 hPa geopotential height over the Northern Hemisphere from A-K31 **(a)**. Ratio of standard deviations from A-K31 and ERA-Interim **(b)**, K-O and ERA-Interim **(c)**, A-K31 and A-Kcl **(d**; impact of SST variability), K-O and A-K31 **(e**; impact of coupling) and K-O and A-Kcl **(f**; impact of both). Changes in variance are only shown where they are significant at the 95 % level.

itude and if both these criteria hold for at least 5 consecutive days. This analysis yields a daily binary 2-D map of persistent quasi-stationary blocked grid points. In the Euro-Atlantic sector atmospheric blocking is most prominent during the winter and spring seasons; the MAM (March-April-May) blocking frequencies for ERA-Interim and the MetUM simulations are shown in Fig. 10.

In the ERA-Interim, there are two maxima in MAM blocking frequency: off the south-west coast of Ireland and over the Baltic region (Fig. 10a). The MetUM is broadly able to represent the spatial pattern of blocking in DJF (not shown) and MAM (Fig. 10) but underestimates the frequency of blocking events. Specifically, A-Kcl does indicate blocking frequency maxima in the correct locations compared with ERA-Interim, although they are considerably weaker than observed. Furthermore, A-Kcl exhibits too much blocking activity over Greenland and Baffin Bay (Fig. 10b). Interannual variability in SST does not improve this bias but further increases blocking activity over Greenland and weakens blocking activity in the observed maxima regions (Fig. 10c). Including near-global air–sea interactions increases the blocking frequency off the south-west coast of Ireland and decreases blocking over Greenland, resulting in a closer-to-observed blocking frequency pattern (Fig. 10d). Interestingly, K-O is not coupled in the seas surrounding Greenland, suggesting the change of blocking frequency there is an impact of non-local coupling. Blocking frequency over the Baltic region remains underestimated in all MetUM simulations. During DJF the MetUM underestimates blocking frequency over the UK and Scandinavia compared with the ERA-Interim; this remains the case even with the introduction of interannual variability in SST and coupling feedbacks (not shown).

This initial analysis suggests that introducing air–sea interactions in K-O changes the distribution and frequency of blocking events in the Northern Hemisphere. With the improved representation of tropical variability associated with the MJO in K-O (Sect. 4.1.2), and the known link between the MJO and extratropical variability (e.g. Cassou, 2008), this is an appropriate modelling framework to investigate the relative roles of local and remote coupling on these modes of variability and the teleconnections linking them (see Sect. 5 for further discussion).

5   Discussion and conclusions

A new coupled modelling framework (MetUM-GOML) has been described in which an AGCM is coupled to a high-resolution, vertically resolved mixed-layer ocean. This is the first coupled system that is capable of providing well-resolved air–sea interactions at limited additional computational expense, enabling high-resolution, climate length integrations.

Four-dimensional temperature and salinity corrections are used to represent ocean advection in the model. Although these corrections need to be prescribed, the model can be constrained to any ocean state to calculate the heat and salt tendencies. Within the experiments described here the model is constrained to observations such that the role of coupling can be investigated within a model with very small SST biases. This controllable feature of the modelling framework, combined with the ability to couple selectively in space and time to any GCM, results in a powerful research tool for process-based studies of the impact of coupling on subseasonal variability.
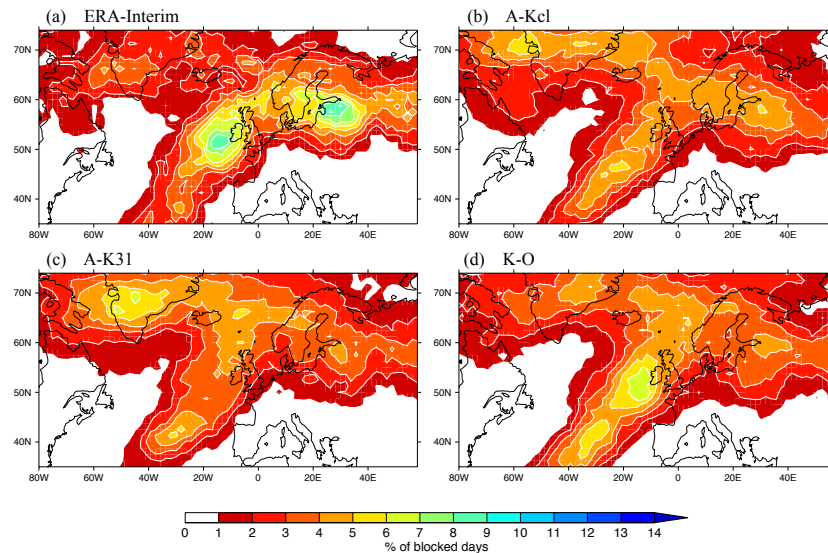
Figure 10. Euro-Atlantic springtime (MAM) blocking frequency climatology using the absolute geopotential height index calculated from the 500 hPa geopotential heights after Tibaldi and Molteni (1990) and Scherrer et al. (2006).

MetUM-GOML simulations were performed (K-O) as well as MetUM atmosphere-only simulations forced by 31-day smoothed SSTs (A-K31) or the mean seasonal cycle of SSTs (A-Kcl) from K-O (Table 1). This allowed the impact of introducing interannual variability in SST (A-K31 minus A-Kcl) to be separated from the impact of coupling feedbacks (K-O minus A-K31). It should be noted that since the K-O SSTs used to force A-K31 have undergone a 31-day smoothing, the latter comparison (K-O minus A-K31) includes the effect of increased, higher frequency SST variability as well as coupling feedbacks.

The performance of these simulations has been assessed by comparing the representation of their mean state and analysing their ability to reproduce several aspects of tropical and extratropical variability. Compared with ERA-Interim reanalysis, the MetUM is shown to be too warm in the stratosphere, too cool and dry in the tropical mid- and lower troposphere and have an equatorward shift in the subtropical jets. Introducing variability in SST is shown to slightly narrow the Southern Hemisphere subtropical jet, while coupling is shown to warm and dry above the boundary layer, cool the upper troposphere and reduce the upper-level equatorial westerly bias. However, all of these tropospheric mean-state changes are small in magnitude (Figs. 3, 4). Larger differences are seen in the representation of tropical precipitation. SST variability reduces precipitation over the equatorial Indian Ocean and maritime continent; coupling reduces (increases) precipitation over the SPCZ and equatorial Indian Ocean (maritime continent). These changes result in a reduction in the long standing equatorial Indian Ocean dry bias (Ringer et al., 2006; Sperber et al., 2013), but have little impact on the lack of monsoonal precipitation over the Indian subcontinent in the MetUM (Fig. 5).

Consistent with the mean-state changes described above, coupling improves the distribution and variability of intraseasonal convection in the tropics (Fig. 7). A detailed examination of convectively coupled equatorial wave modes indicates that all the MetUM simulations underestimate or, in some cases, fail to capture the variability corresponding to observed wave modes. Coupling is shown to concentrate the eastward power associated with the MJO and reduce spurious low-frequency westward power (Fig. 6). In fact, the propagation of the MJO is significantly improved in K-O; coupling feedbacks transform the MJO signal from stationary or westward propagating precipitation anomalies in A-K31 to a clear eastward propagating signal. This MJO signal, however, remains weaker than in observations (Fig. 8).

The influence of air–sea coupling has also been examined in the extratropics. In the MetUM, the Northern Hemisphere Pacific storm track is too weak and the Atlantic track does not extend far enough into Europe. Introducing interannual variability in SST broadens the area of strong eddy activity in the Pacific but coupling has little impact on the storm tracks in either basin (Fig. 9). However, coupling feedbacks do appear to slightly improve the frequency of atmospheric blocking over the Euro-Atlantic sector, although this remains lower than observed (Fig. 10).

In terms of the diagnostics considered here, MetUM-GOML has generally been shown to slightly improve the representation of tropical and extratropical variability compared with its atmosphere-only counterpart. With a more accurate representation of variability, this framework could be used as a test bed for investigating how global weather and climate extremes may change in a warming world.

Despite its known limitation of being unable to produce dynamically driven oceanic variability, this framework pro-

vides a new and exciting research tool for process-based studies of air–sea interactions. The limited computational cost enables coupling to be applied at higher GCM horizontal resolution; the current framework has also been implemented with the MetUM at horizontal resolutions of ∼ 60 and ∼ 25 km (the simulations described here are ∼135 km resolution). Results from these integrations will form the basis of future studies. Furthermore, the technical advantages described in Sect. 1.3 present many opportunities for further sensitivity studies. The controllability of this framework, for example, could be used to constrain the ocean to a particular mode of variability from interannual (ENSO) and decadal (PDO) to multi-decadal (AMO) timescales to investigate the role coupling plays in the teleconnection patterns associated with that pattern of oceanic variability. Alternatively, by constraining MC-KPP to a model ocean climatology, MetUM-GOML could be used to investigate the role of regional SST biases. Within coupled simulations using a full dynamical ocean, changes in the coupled mean state are often compensated by large biases in the coupled system. With this framework, the impact of particular regional SST biases could be investigated remaining within a framework that represents air–sea interactions. Furthermore, the adaptable nature of the framework could be exploited to selectively couple (or uncouple) in local regions of interest to investigate the relative role of local and remote air–sea interactions on various atmospheric phenomena. As a research tool, this new coupled modelling framework will be applied in many future contexts and studies.

Code availability

The source code for MC-KPP version 1.0 is available in the subversion repository at https://puma.nerc.ac.uk/svn/KPP_ocean_svn/KPP_ocean/tags/MC-KPP_vn1.0. Further description and information about the MC-KPP model is available at https://puma.nerc.ac.uk/trac/KPP_ocean and further information regarding MetUM-GOML is available at https://puma.nerc.ac.uk/trac/KPP_ocean/wiki/MetUM-GOML.

References

Alexander, M. A., Scott, J. D., and Deser, C.: Processes that influence sea surface temperature and ocean mixed layer depth variability in a coupled model, J. Geophys. Res, 105, 16823–16842, 2000.

Arribas, A., Glover, M., Maidens, A., Peterson, K., Gordon, M., MacLachlan, C. D., Fereday, R. G., Camp, J., Scaife, A. A., Xavier, P., Coleman, A., and Cusack, S.: The GloSea4 ensemble prediction system for seasonal forecasting, Mon. Weather Rev., 139, 1891–1910, 2011.

Benedict, J. J. and Randall, D. A.: Impacts of Idealized Air-Sea coupling on Madden-Julian Oscillation sctructure in the Super-parameterized CAM, J. Atmos. Sci., 68, 1990–2008, 2011.

Bernie, A. J., Guilyardi, E., Madec, G., Slingo, J. M., Woolnough, S. J., and Cole, J.: Impact of resolving the diurnal cycle in an ocean-atmosphere GCM. Part 2: A diurnally coupled CGCM, Clim. Dynam., 31, 909–925, 2008.

Bhatt, U. S., Alexander, M. A., Battisti, D. S., Houghton, D. D., and Keller, L. M.: Atmosphere-Ocean Interaction in the North Atlantic: Near-Surface Climate Variability, J. Climate, 11, 1615–1632, 1998.

Blackmon, M. L.: A Climatological Spectral Study of the 500 mb Geopotential Height of the Northern Hemisphere, J. Atmos. Sci., 33, 1607–1623, 1979.

Cassou, C.: Intraseasonal interaction between the Madden-Julian Oscillation and the North Atlantic Oscillation, Nature, 455, 523–527, 2008.

Cassou, C., Terray, L., and Phillips, A. S.: Tropical Atlantic Influence on European Heat Waves, J. Climate, 18, 2805–2811, 2005.

Cassou, C., Deser, C., and Alexander, M. A.: Investigating the Impact of Reemerging Sea Surface Temperature Anomlaies on the Winter Atmospheric Circulation over the North Atlantic, J. Climate, 20, 3510–3526, 2007.

Crueger, T., Stevens, B., and Brokopf, R.: The Madden-Julian Oscillation in ECHAM6 and the introduction of an objective MJO Index, J. Climate, 26, 3241–3257, 2013.

Dee, D. P., Uppala, S. M., Simmons, A. J., Berrisford, P., Poli, P., Kobayashi, S., Andrae, U., Balmaseda, M. A., Balsamo, G., Bauer, P., Bechtold, P., Beljaars, A. C. M., van de Berg, L., Bidlot, J., Bormann, N., Delsol, C., Dragani, R., Fuentes, M., Geer, A. J., Haimberger, L., Healy, S. B., Hersbach, H., Holm, E. V., Isaksen, L., Kallberg, P., Kohler, M., Matricardi, M., McNally, A. P., Monge-Sanz, B. M., Morcrette, J.-J., Park, B.-K., Peuby, C., de Rosnay, P., Tavolato, C., Thepaut, J.-N., and Vitart, F.: The ERA-Interim reanalysis: configuration and performance of the data assimilation system, Q. J. Roy. Meteorol. Soc., 137, 553–597, 2011.

DeMott, C. A., Stan, C., Randall, D. A., and Branson, M. D.: Intraseasonal Variability in Coupled GCMs: The Roles of Ocean Feedbacks and Model Physics, J. Climate, 27, 4970–4995, 2014.

Doblas-Reyes, F., Casado, M. J., and Pastor, M. A.: Sensitivity of the Northern Hemisphere blocking frequency to the detection index, J. Geophys. Res., 107, ACL6.1–ACL.6.22, doi:10.1029/2000JD000290, 2002.

Feudale, L. and Shukla, J.: Influence of sea surface temperature on the European heat wave of 2003 summer. Part I: an observational study, Clim. Dynam., 36, 1691–1703, 2011.

Fu, X., Wang, B., Li, T., and McCreary, J. P.: Coupling between Northward-Propagating, Intraseasonal Oscillations and Sea Sur-

face Temperature in the Indian Ocean, J. Atmos. Sci., 60, 1733–1753, 2003.

Giannini, A., Saravanan, R., and Chang, P.: Oceanic Forcing of Sahel Rainfall on Interannual to Interdecadal Time Scales, Science, 302, 1027–1030, 2003.

Guemas, V., Salas-Mèlia, D., Kageyama, M., Giordani, H., and Voldoire, A.: Impact of the ocean diurnal cycle on the North Atlantic mean sea surface temperatures in a regionally coupled model, Dynam. Atmos. Oceans., 60, 28–45, 2013.

Ham, Y.-G. and Kug, J.-S.: Impact of diurnal atmosphere-ocean coupling on tropical climate simulations using a coupled GCM, Clim. Dynam., 34, 905–917, 2010.

Hendon, H. H. and Liebmann, B.: The Intraseasonal (30–50 day) Oscillation of the Australian Summer Monsoon, J. Atmos. Sci., 47, 2909–2923, 1990.

Hendon, H. H., Lim, E.-P., and Luo, G.: The Role of Air-Sea Interaction for Prediction of Australian Summer Monsoon Rainfall, J. Climate, 25, 1278–1290, 2012.

Hoskins, B. J. and Hodges, K. I.: New Perspectives on the Northern Hemisphere Winter Storm Tracks, J. Atmos. Sci., 59, 1041–1061, 2002.

Inness, P. M., Slingo, J. M., Guilyardi, E., and Cole, J.: Simulation of the Madden-Julian Oscillation in a Coupled General Circulation Model: Part II: The Role of the Basic State, J. Climate, 16, 365–382, 2003.

Jullien, S., Marchesiello, P., Menkes, C. E., Lefévre, J., Jourdain, N. C., Samson, G., and Lengaigne, M.: Ocean feedback to tropical cyclones: climatology and processes, Clim. Dynam., 43, 2831–2854, 2014.

Kim, D., Sperber, K., Stern, W., Waliser, D., Kang, I.-S., Maloney, E. D., Wang, W., Weickmann, K. J., Benedict, M. K., Lee, M.-I., Neale, R., Suarez, M., Thayer-Calder, K., and Zhang, G.: Application of MJO Simulation Diagnostics to Climate Models, J. Climate, 22, 6413–6436, 2009.

Klingaman, N. P. and Woolnough, S. J.: The Role of air–sea coupling in the simulation of the Madden-Julian oscillation in the Hadley Centre model, Q. J. Roy. Meteorol. Soc., 140, 2272–2286, doi:10.1002/qj.2295, 2014.

Klingaman, N. P., Woolnough, S. J., Weller, H., and Slingo, J. M.: The Impact of Finer-Resolution Air-Sea Coupling on the Intraseasonal Oscillation of the Indian Monsoon, J. Climate, 24, 2451–2468, 2011.

Kummerow, C., Barnes, W., Kozu, T., Shiue, J., and Simpson, J.: The Tropical Rainfall Measuring Mission (TRMM) sensor package, J. Atmos. Ocean. Tech., 15, 809–817, 1998.

Kwon, Y.-O., Deser, C., and Cassou, C.: Coupled atmosphere-mixed layer ocean response to ocean heat flux convergence along the Kuroshio Current Extension., Clim. Dynam., 36, 2295–2312, 2011.

Large, W., McWilliams, J., and Doney, S.: Oceanic vertical mising: A review and a model with a nonlocal boundary layer parameterization, Rev. Geophys., 32, 363–403, 1994.

Lavender, S. L. and Matthews, A. J.: Response of the West African Monsoon to the Madden-Julian Oscillation, J. Climate, 22, 4097–4116, 2009.

Lawrence, D. M. and Webster, P. J.: The Boreal Summer Intraseasonal Oscillation: Relationship between Northward and Eastward Movement of Convection, J. Atmos. Sci., 59, 1593–1606, 2002.

Madden, R. A. and Julian, P. R.: Detection of a 40–50 Day Oscillation in the Zonal Wind in the Tropical Pacific, J. Atmos. Sci., 28, 702–708, 1971.

Madden, R. A. and Julian, P. R.: Description of Global-Scale Circulation Cells in the Tropics with a 40-50 Day Period, J. Atmos. Sci., 29, 1109–1123, 1972.

Maloney, E. D. and Sobel, A. H.: Surface Fluxes and Ocean Coupling in the Tropical Intraseasonal Oscillation, J. Climate., 17, 4368–4386, 2004.

Martin, G. M., Dearden, C., Greeves, C., Hinton, T., Inness, P., James, P., Pope, V., Ringer, M., Slingo, J. M., Stratton, R., and Yang, G.-Y.: Evaluation of the atmospheric performance of HadGAM/GEM1, Tech. Rep. 54, Hadley Centre Tech. Note, 2004.

Matthews, A. J.: Intraseasonal Variability over Tropical Africa during Northern Summer, J. Climate, 17, 2427–2440, 2004.

Nakamura, M. and Yamane, S.: Dominant Anomaly Patterns in the Near-Surface Baroclinicity and Accompanying Anomalies in the Atmosphere and Oceans. Part I: North Atlantic Basin, J. Climate, 22, 880–904, 2009.

Neelin, J. D., Battisti, D. S., Hirst, A. C., Jin, F.-F., Wakata, Y., Yamagata, T., and Zebiak, S. E.: ENSO theory, J. Geophys. Res, 103, 14261–14290, 1998.

Pezza, A. B., van Rensch, P., and Cai, W.: Severe heat waves in Southern Australia: synoptic climatology and large scale connections, Clim. Dynam., 38, 209–224, 2012.

Prodhomme, C., Terray, P., Masson, S., Boschat, G., and Izumo, T.: Oceanic factors controlling the Indian summer monsoon onset in a coupled model, Clim. Dynam., 2014.

Rajendran, K. and Kitoh, A.: Modulation of Tropical Intraseasonal Oscillations by Ocean-Atmosphere Coupling, J. Climate, 19, 366–391, 2006.

Rajendran, K., Kitoh, A., and Arakawa, O.: Monsoon low-frequency inrtaseasonal oscillation and ocean-atmosphere coupling over the Indian Ocean, Geophys. Res. Lett., 31, L02210, doi:10.1029/2003GL019031, 2004.

Ray, P., Zhang, C., Moncrieff, M. W., Dudhia, J., Caron, J. M., Leung, L. R., and Bruyere, C.: Role of the atmospheric mean state on the initiation of the Madden-Julian Oscillation in a tropical channel model, Clim. Dynam., 36, 161–184, 2011.

Ringer, M. A., Martin, G. M., Greeves, C. Z., Hinton, T. J., James, P. M., Pope, V. D., Scaife, A. A., Stratton, R. A., Inness, P. M., Slingo, J. M., and Yand, G.-Y.: The Phyiscal Properties of the Atmosphere in the New Hadley Centre Global Environmental Model (HadGEM1). Part II: Aspects of Variability and Regional Climate, J. Climate, 19, 1302–1326, 2006.

Sandery, P. A., Brassington, G. B., Craig, A., and Pugh, T.: Impacts of ocean-atmosphere coupling on tropical cyclone intensity change and ocean prediction in the Australian region., Mon. Weather Rev., 138, 2074–2091, 2010.

Sausen, R., Barthel, K., and Hasselmann, K.: Coupled ocean-atmosphere models with flux corrections, Clim. Dynam., 2, 145–163, 1988.

Scaife, A. A., Woolings, T., Knight, J. R., Martin, G., and Hinton, T.: Atmospheric blocking and mean biases in climate models, J. Climate, 23, 6143–6152, 2010.

Scherrer, S. C., Croci-Maspoli, M., Schwierz, C., and Appenzeller, C.: Two-Dimensional indicies of Atmospheric Blocking and

their statistical relationship with wither climate pattens in the Euro-Atlantic region, Int. J. Climatol., 26, 233–249, 2006.

Seo, K.-H., Schemm, J.-K. E., Wang, W., and Kumar, A.: The Boreal Summer Intraseasonal Oscillation Simulated in the NCEP Climate Forecast System: The Effect of Sea Surface Temperature, Mon. Weather Rev., 135, 1807–1827, 2007.

Shinoda, T., Jensen, T. G., Flatau, M., Chen, S., Han, W., and Wang, C.: Large-Scale Oceanic Variability Associaed with the Madden-Julian Oscillation during the CINDY/DYNAMO Field Campaign from Satellite Observations, Remote Sens., 5, 2072–2092, 2013.

Smith, D. M. and Murphey, J. M.: An objective ocean temperature and salinity analysis using covariances from global climate models, J. Geophys. Res., 112, C02022, doi:10.1029/2005JC003172, 2007.

Smith, W. H. F. and Sandwell, D. T.: Global Sea Floor Topography from Satellite Altimetry and Ship Depth Soundings, Science, 277, 1956–1962, 1997.

Sperber, K. R., Annamalai, H., Kang, L.-S., Kitoh, A., Moise, A., Turner, A., Wang, B., and Zhou, T.: The Asian summer monsoon: an intercomparison of CMIP5 vs. CMIP3 simulations of the late 20th century, Clim. Dynam., 41, 2711–2744, 2013.

Straub, K. H. and Kiladis, G. N.: Extratropical forcing of convectively coupled Kelvin waves during austral winter, J. Atmos. Sci., 60, 526–543, 2003.

Sutton, R. T. and Hodson, D. L. R.: Influences of the Ocean on North Atlantic Climate Variability 1871–1999, J. Climate., 16, 3296–3313, 2003.

Sutton, R. T. and Hodson, D. L. R.: Atlantic Ocean Forcing of North American and European Summer Climate, Science, 309, 115–118, 2005.

Taylor, K. E., Stouffer, R. J., and Meehl, G. A.: An Overview of CMIP5 and the Experiment Design, B. Am. Meteorol. Soc., 93, 485–498, 2012.

Tibaldi, S. and Molteni, F.: On the operational predictability of blocking, Tellus, 42A, 343–365, 1990.

Tseng, W.-L., Tsuang, B.-J., Keenlyside, N. S., Hsu, H.-H., and Tu, C.-Y.: Resolving the upper-ocean warm layer improves the simulation of the Madden-Julian oscillation, Clim. Dynam., 112, 1–17, doi:10.1007/s00382-014-2315-1, 2014.

Valcke, S., Caubel, A., Declat, D., and Terray, L.: OASIS3 Ocean Atmosphere Sea Ice Soil user's guide, Tech. Rep. TR/CMGC/03/69, CERFACS, Toulouse, France, 2003.

Vannière, B., Guilyardi, E., Madec, G., Doblas-Reyes, F., and Woolnough, S. J.: Using seasonal hindcasts to understand the origin of the equatorial cold toungue bias in CGCMs and its impact on ENSO, Clim. Dynam., 40, 963–981, 2012.

Vecchi, G. A. and Harrison, D. E.: Monsoon breaks and subseasonal sea surface temperature variability in the Bay of Bengal, J. Climate, 15, 1485–1493, 2002.

Vitart, F.: Impact of the Madden Julian Oscillation on tropical storms and risk of landfall in the ECMWF forecast system, Geophys. Res. Lett., 36, L15802, doi:10.1029/2009GL039089, 2009.

Vitart, F. and Molteni, F.: Dynamical Extended-Range Prediction of Early Monsoon Rainfall over India, Mon. Weather Rev., 137, 1480–1492, 2009.

Vitart, F. and Molteni, F.: Simulation of the MJO and its teleconnections in the ECMWF forecast system, Q. J. Roy. Meteorol. Soc., 136, 842–855, 2010.

Walters, D. N., Best, M. J., Bushell, A. C., Copsey, D., Edwards, J. M., Falloon, P. D., Harris, C. M., Lock, A. P., Manners, J. C., Morcrette, C. J., Roberts, M. J., Stratton, R. A., Webster, S., Wilkinson, J. M., Willett, M. R., Boutle, I. A., Earnshaw, P. D., Hill, P. G., MacLachlan, C., Martin, G. M., Moufouma-Okia, W., Palmer, M. D., Petch, J. C., Rooney, G. G., Scaife, A. A., and Williams, K. D.: The Met Office Unified Model Global Atmosphere 3.0/3.1 and JULES Global Land 3.0/3.1 configurations, Geosci. Model Dev., 4, 919–941, doi:10.5194/gmd-4-919-2011, 2011.

Wang, W., Chen, M., and Kumar, A.: Impacts of Ocean Surface on the Northward Propagation of the Boreal Summer Intraseasonal Oscillation in the NCEP Climate Forecast System, J. Climate, 22, 6561–6576, 2009.

Watterson, I. G.: The sensitivity of subannual and intraseasonal tropical variability to model ocean mixed layer depth, J. Geophys. Res., 107, ACL12.1–ACL12.15, 2002.

Wheeler, M. C. and Hendon, H. H.: An All-Seasonal Real-Time Multivariate MJO Index: Development of an Index for Monitoring and Prediction, Mon. Weather Rev., 132, 1917–1932, 2004.

Wheeler, M. C. and Kiladis, G. N.: Convectively Coupled Equatorial Waves: Analysis of Clouds and Temperature in the Wavenumber-Frequency Diagram, J. Atmos. Sci., 56, 374–399, 1999.

Woolnough, S. J., Vitart, F., and Balmaseda, M. A.: The role of the ocean in the Madden-Julian Oscillation: Implications for MJO prediction, Q. J. Roy. Meteorol. Soc., 133, 117–128, 2007.

Wu, G., Guan, Y., and Liu, Y.: Air-sea interaction and formation of the Asian summer monsoon onset vortex over the Bay of Bengal, Clim. Dynam., 38, 261–279, 2012.

Zhang, C.: Madden-Julian Oscillation, Rev. Geophys., 43, RG2003, doi:10.1029/2004RG000158, 2005.